ACS Sustainable Chemistry & Engineering

Research Article

pubs.acs.org/journal/ascecg

Graphene-Analogue Hexagonal BN Supported with Tungsten-based Ionic Liquid for Oxidative Desulfurization of Fuels

Wenshuai Zhu,*[,†] Bilian Dai,[†] Peiwen Wu,[‡] Yanhong Chao,[†] Jun Xiong,[†] Suhang Xun,[†] Hongping Li,[†] and Huaming Li*[,§]

[†]School of Chemistry and Chemical Engineering, Jiangsu University, 301 Xuefu Road, Zhenjiang 212013, People's Republic of China

[‡]School of Energy and Power Engineering, Jiangsu University, 301 Xuefu Road, Zhenjiang 212013, People's Republic of China

[§]Insititute for Energy Research, Jiangsu University, 301 Xuefu Road, Zhenjiang 212013, People's Republic of China

Supporting Information

ABSTRACT: Graphene-analogue hexagonal boron nitride (G-*h*-BN), as a novel few-layer material, was prepared and used as a support to coat with tungsten-based ionic liquid (IL) in oxidative desulfurization. Designed G-*h*-BN supported with tungsten-based IL (IL/G-*h*-BN) heterogeneous catalyst was characterized by atomic force microscopy, scanning electron microscopy, energy-dispersive X-ray spectroscopy, transmission electron microscopy, X-ray diffraction, Raman and X-ray photoelectron spectroscopy. This few-layer material supported with IL strategy makes the usage amount of IL reduce remarkably, which not only presents excellent catalytic activity but also is superior to homogeneous catalysts of ILs themselves. Additionally, compared with the multilayer hexagonal boron nitrides (M-*h*-BN) or commercial bulk BN supported with IL, the IL/G-*h*-BN catalyst exhibited better catalytic activity in oxidation of dibenzothiophene, reaching 99.3% sulfur removal. The adsorption and catalytic oxidative desulfurization mechanism was further studied by gas chromatography−mass spectrometry, Fourier transform infrared spectroscopy, X-ray diffraction and UV-diffuse reflectance spectroscopy. Moreover, the IL/G-*h*-BN catalyst could be recycled five times with little decrease in catalytic activity.

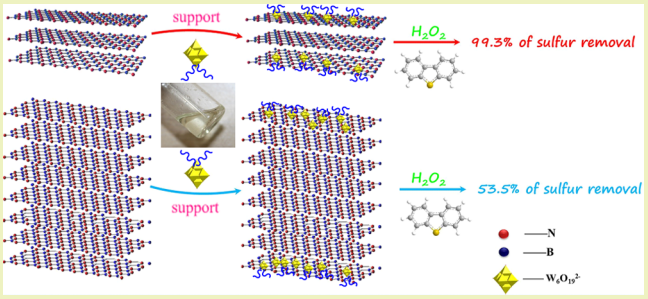

KEYWORDS: *Oxidative desulfurization, ionic liquid, graphene-analogue, boron nitride, heterogeneous catalysis*

INTRODUCTION

Ionic liquids (ILs), as liquid ion compounds, have been extensively used as solvents in organic reactions.[1−4] To enlarge the range of the applications of ILs, task-specific ILs are developed not only as solvents but also as catalysts.[5−7] In recent years, task-specific ILs have been widely applied in oxidation of starch,[8] epoxidation of alkenes,[9] hydrogenation of carbon dioxide,[10] adsorption of SO_2,[11] desulfurization,[12−18] etc. Although these biphasic reactions occurring in task-specific ILs exhibit good catalytic activity, they still suffer from some disadvantages, such as high cost and large usage amount of ILs,[19,20] imposing restrictions on the development of ILs. To overcome these limitations, heterogeneous solid catalyst, supported IL phase materials have been introduced because they not only decrease the cost and the usage amount of ILs but also facilitate separation and utilization in a supported-bed reactor.[5,7,21−24] However, most of the heterogeneous catalysts have a lower catalytic ability than homogeneous IL catalysts because of the lower exposure degree of the catalytic sites. Xiao et al.[25] found that heterogeneous catalysts of ILs functionalized on superhydrophobic mesoporous polymers could exhibit much higher activities in transesterification than homogeneous catalysts of the ILs themselves.[22] Therefore, it is important to choose an appropriate support to increase the catalytic activity of heterogeneous supported IL catalysts.

By now, silica gel,[26] mesoporous silica,[27−29] alumina,[30] carbon nanotubes,[31] MgO,[32] metal organic frameworks,[33] etc. supports have been used to immobilize ILs. However, different supports have their own shortages. For instance, the specific surface area of oxides (MgO) is very small, causing low efficiency of supporting. Though porous materials have large specific surface areas, the pores of porous materials would be blocked and aggregated easily, leading to recycling difficulties. Therefore, it is a vital key to develop a support with large specific surface area, high activity and recyclability. Graphene-analogue hexagonal boron nitride (G-*h*-BN), as a novel few-layer material, has attracted increasingly attention due to its special layered structure and large Brunauer−Emmett−Teller (BET) surfaces[34−37] and special sp^2-bonded layered feature of G-*h*-BN presents outstanding durability and adsorption capacity, indicating that it is a good structural supportive material in series of potential applications.[38−40] Task-specific

Received: November 4, 2014
Revised: November 26, 2014
Published: December 4, 2014

dx.doi.org/10.1021/sc5006928 | ACS Sustainable Chem. Eng. 2015, 3, 186−194

ILs can disperse highly onto large BET surfaces G-*h*-BN, showing remarkable synergetic adsorption effects to enhance the catalytic activity of ILs. By this way, a greatly dispersed, high active, easily reusable catalyst can be obtained. As a layered material, the number of layers of *h*-BN has an important effect on its specific surface area, further affecting the loading efficiency and catalytic activity.

Oxidation of aromatic sulfides is an important reaction due to the promising potential applications in oxidative desulfurization of fuels.[41−51] Aromatic sulfides can be oxidized selectively to sulfoxides and sulfones, which can be removed by polar extractants or adsorbents. In this way, ultralow sulfur fuels can be achieved.[52−54] Here, a tungsten-based task-specific IL $[(C_6H_{13})_3PC_{14}H_{29}]_2W_6O_{19}$ was highly dispersed on G-*h*-BN to obtain G-*h*-BN supported with ionic liquid (IL/G-*h*-BN) catalyst. This as-prepared heterogeneous IL/G-*h*-BN catalyst showed high catalytic activity in oxidative desulfurization, which can be attributed to the following reasons. (1) G-*h*-BN as a novel few-layer support with large BET surfaces is beneficial for the dispersion of ILs. (2) Large BET surfaces of G-*h*-BN are responsible for excellent adsorptive performance to substrates and oxidant, which can form a microenvironment with high concentration of reaction system on the surface of the catalyst. So, compared with the homogeneous catalysts of ILs, this few-layer material supported with IL strategy presents excellent catalytic activity, which not only makes the usage amount of tungsten-based IL, the reaction temperature and hydrogen peroxide consumption decrease remarkably, but also surpasses the catalytic activity of solely homogeneous ILs themselves. Moreover, the IL/G-*h*-BN exhibited much higher desulfurization than multilayer *h*-BN (M-*h*-BN) and commercial available BN supported with ionic liquid catalysts. The as-prepared catalyst could be separated easily by centrifugation and recycled five times without significant decrease in catalytic activity.

EXPERIMENTAL SECTION

Materials. Boric acid (H_3BO_3, AR grade), urea ($CO(NH_2)_2$, AR grade), hydrogen peroxide (H_2O_2, 30 wt %), methylene chloride (CH_2Cl_2, AR grade) and *n*-octane (AR grade) were purchased from Shanghai Sinopharm Chemical Reagent Co., Ltd. and used without purification. $[(C_6H_{13})_3PC_{14}H_{29}]Cl$ (99%), dibenzothiophene (DBT, 98%), thianaphthene (BT, 99%), 4,6-dimethyldibenzothiophene (4,6-DMDBT, 97%) and tetradecane (99%) were purchased from Sigma-Aldrich without purification.

Preparation of Catalyts. *Synthesis of Few-Layer G-h-BN.* Boric acid and urea with a molar ratio (1:24) were dissolved in 40 mL of ultrapure water. The solution was heated at 65 °C until the water was evaporated completely. The mixtures were heated at 5 °C/min from room temperature to 900 °C in N_2 atmosphere and remained 2 h to get the G-*h*-BN product.[55] Multilayer M-*h*-BN was prepared in the similar procedure only changing the different molar ratio (1:12) of boric acid and urea.

Synthesis of Tungsten-based IL. 8.25 g of $Na_2WO_4{\cdot}2H_2O$ was stirred in an acetic anhydride (10 mL)−dimethylformamide (7.5 mL) mixture for 3 h at 100 °C. A mixture of acetic anhydride (5 mL), dimethylformamide (12.5 mL) and concentrated hydrochloric acid (4.5 mL) was then added. After 2 h at 100 °C, the white residue was filtered. The solution was decanted after reacting with 5.84 g of $[(C_6H_{13})_3PC_{14}H_{29}]Cl$, and $[(C_6H_{13})_3PC_{14}H_{29}]_2W_6O_{19}$ was left at the bottom. The crude liquid product was washed out by acetonitrile, whose melting point is −48 °C.[56]

Synthesis of IL/G-h-BN and IL/M-h-BN Catalysts. To get G-*h*-BN and M-*h*-BN supported with IL, IL and BN (G-*h*-BN, M-*h*-BN and commercial available BN) with a mass ratio 1:9 were mixed in methylene chloride and stirred for 3 h at room temperature and dried in vacuum at 110 °C. The as-prepared G-*h*-BN and M-*h*-BN supported with IL were denoted as IL/G-*h*-BN, IL/M-*h*-BN and IL/commercial available BN, respectively.

Desulfurization of Model Oil. Different model oils were prepared as follows: DBT, BT and 4,6-DMDBT were dissolved in *n*-octane to form model oils with the corresponding S-content of 500, 250 and 250 ppm, respectively.

In a typical oxidative desulfurization process, after a required amount of catalyst was added to a homemade 40 mL two-necked flask, 30 wt % H_2O_2 and 5 mL model oil were poured into the flask, and then the mixed solution was stirred vigorously in a thermostatic water-bath. After the reaction, the upper liquid phase samples were periodically withdrawn and separated by centrifugation before sulfur content was analyzed. The oil sample was analyzed on a gas chromatography flame ionization detection (GC-FID, Agilent 7890A, HP-5 column, 30 m long × 0.32 mm inner diameter (id) 0.25 μm film thickness) instrument with tetradecane as an internal standard. The process started at 100 °C and the temperature was increased to 200 °C at the rate of 15 °C·min^{-1}. Sulfur removal in model oil was used to figure the conversion of DBT.

Characterization methods. Fourier transform infrared spectroscopy (FT-IR) spectra of the reactants and the products were obtained on a Nicolet Nexus 470 Fourier transform infrared spectrometer, using KBr pellets at room temperature. Ultraviolet−visible diffuse reflectance spectrosopy (UV−DRS) measurements were recorded on a Shimadzu UV-2450 spectrophotometer equipped with spherical diffuse reflectance accessory in the range of 200−800 nm, using $BaSO_4$ as the reflectance standard material. The surface morphologies of samples were analyzed by field emission scanning electron microscopy (SEM, Leo Supra 35VP), which was performed at 2−15 keV accelerating voltage. An energy-dispersive X-ray (EDS) analyzing system was used to conduct the elemental analysis. X-ray photoelectron spectroscopy (XPS) spectra were recorded on a ESCALAB250 (Thermo VG, UK), in which standard monochromatic Al Kα excitation was 1486.6 eV. Raman tests were carried out using Thermo Scientific DXR Smart Raman spectrometer equipped with a 532 nm excitation. The shape of *h*-BN and the appearance of IL/*h*-BN were observed by transmission electron microscopy (TEM, Hitachi H-700). The crystalline phase was measured by X-ray diffraction (XRD) using a D8 ADVANCE X-ray diffraction equipped with Cu Kα radiation (λ) 1.5406 (Å), employing a scanning rate of 0.02° s^{-1} in the 2θ range from 10 to 90°. Atomic force microscopy (AFM) was applied to investigate the layers of *h*-BN. Brunauer−Emmett−Teller (BET) analysis was employed to calculate the specific surface area of *h*-BN and IL/*h*-BN. Meanwhile, gas chromatography−mass spectrometry (GC−MS) was taken to research the mechanism of adsorption coupled with oxidative desulfurization.

RESULTS AND DISCUSSION

Characterizations of Catalysts. Atomic force microscopy (AFM) was performed in order to prove the layers of G-*h*-BN were less than those of M-*h*-BN. AFM images of G-*h*-BN and M-*h*-BN are shown in Figure 1, and thickness of G-*h*-BN and M-*h*-BN was about 3 and 8 nm, respectively. This result indicated that as-prepared *h*-BN had different layers, which may

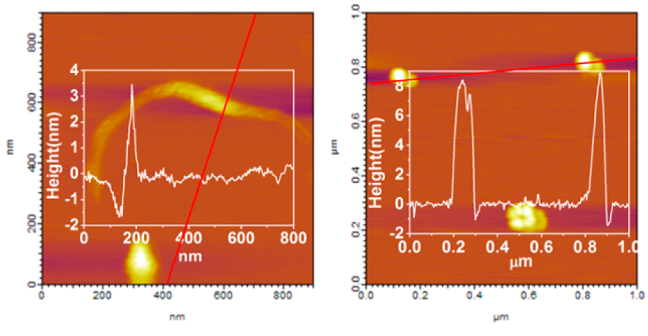

Figure 1. AFM images of G-*h*-BN and M-*h*-BN.

dx.doi.org/10.1021/sc5006928 | ACS Sustainable Chem. Eng. 2015, 3, 186−194

lead to different specific surface areas. So, the BET surface areas of the G-*h*-BN, IL/G-*h*-BN, M-*h*-BN and IL/M-*h*-BN samples were done in order to prove this speculation. Their values were 167.0, 62.5, 53.9 and 26.4 m^2/g, respectively. It can be concluded that the specific surface area increased with the decrease of layers of *h*-BN. Moreover, when IL was supported onto *h*-BN, the specific surface area of *h*-BN decreased, which may result from the formation of IL layered thin film on the surface of *h*-BN, causing the aggregation of *h*-BN powder.

Scanning electron microscopy (SEM) and energy-dispersive X-ray spectroscopy (EDS) analyses of G-*h*-BN and IL/G-*h*-BN were carried out to investigate the surface morphologies and the elemental composition (Figure 2). As shown in Figure 2a,

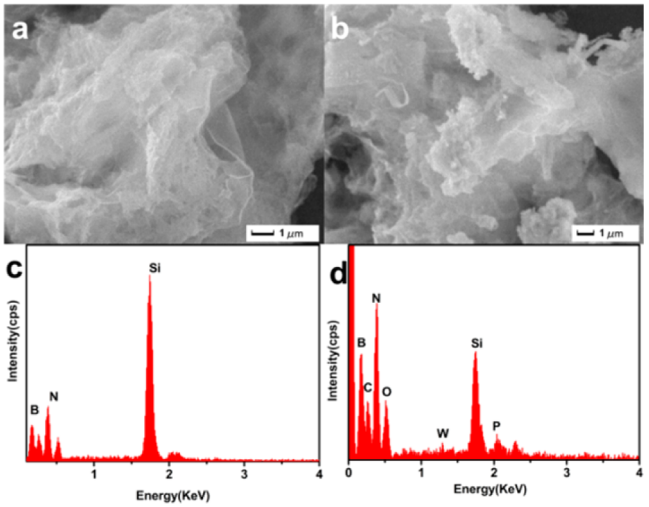

Figure 2. SEM image and EDS analysis of G-*h*-BN (a, c) and IL/G-*h*-BN (b, d).

G-*h*-BN presented a typical structure of graphene-analogue material. The structure of IL/G-*h*-BN was similar to that of G-*h*-BN (Figure 2b). As shown in Figure 2c, only B and N exist in G-*h*-BN, while B, N, C, P, W and O can be found in IL/G-*h*-BN, which proved G-*h*-BN (Figure 2d), supported with tungsten-based IL successfully.

X-ray photoelectron spectroscopy (XPS) is employed to investigate the compositions and element chemical states of IL/G-*h*-BN and exhibited in Figure 3a. All elements B, N, O, C, W and P in IL/G-*h*-BN were detected in the XPS spectrum. The binding energies for B 1s and N 1s peaks were 190.30 and 397.94 eV, respectively (Figure 3b and Figure 3c). These values matched with previous report for *h*-BN,[40,57] which indicated that the synthesized BN may be hexagonal phase.[53] Raman spectra of G-*h*-BN and IL/G-*h*-BN were displayed in Figure 3d. They presented the sharp peak at 1374.2 cm^{-1}, which was contributed to B−N vibrational mode (E_{2g}) within G-*h*-BN layer.[58] Compared with previous report of bulk *h*-BN E_{2g} (1370.9 cm^{-1}), the E_{2g} mode of G-*h*-BN shifted to a higher frequency, proving that the as-prepared *h*-BN was few-layered *h*-BN.[58,59] It also can be seen from Figure 3d that the E_{2g} value of IL/G-*h*-BN was the same as that of G-*h*-BN, demonstrating that the structure of G-*h*-BN was intact after G-*h*-BN was supported with IL.

Transmission electron microscopy (TEM) analysis of G-*h*-BN is presented in Figure 4a, indicating that the as-prepared G-*h*-BN was of the graphene-like structure. Meanwhile, a TEM image of IL/G-*h*-BN in Figure 4b demonstrated the structure of

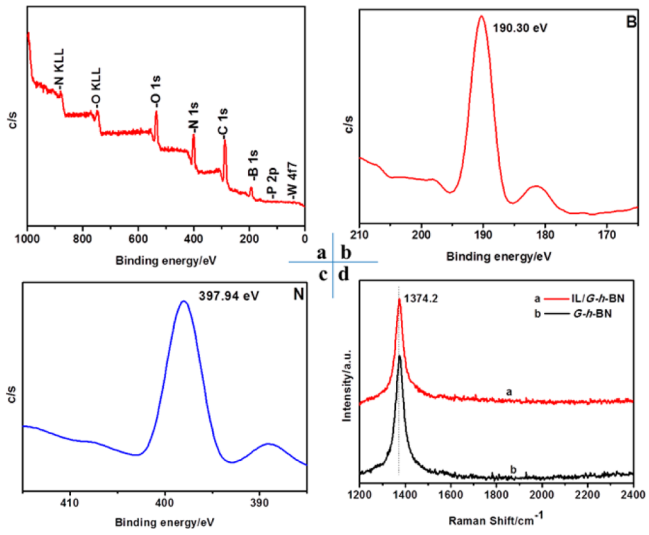

Figure 3. XPS and Raman spectra of G-*h*-BN and IL/G-*h*-BN XPS spectrum of IL/G-*h*-BN; (b, c) XPS spectra of B and N 1s core level, respectively; (d) Raman spectra of G-*h*-BN and IL/G-*h*-BN.

IL/G-*h*-BN remained to be a layered structure. Figure 4c is high resolution (HRTEM) image of Figure 4a. It indicates that *h*-BN is the overlayer with few layers (4−8 layers). Figure 4d is the fast Fourier transform (FFT) image of Figure 4c. It can be seen that the G-*h*-BN was with a polycrystalline structure. In the FFT image, two lattice planes, which were ⟨002⟩ lattice and ⟨100⟩ could be found. A layer-to-layer distance (⟨002⟩ lattice) was 0.349 nm, a little larger than the ⟨002⟩ interplanar distance in bulk *h*-BN[34] due to surface atom relaxation. Such result was further confirmed by XRD patterns (Figure 4f) with a deduced lattice parameter d_{002} = 0.348 nm. The obtained inplane lattice spacing (d_{100} = 0.215 nm) in HRTEM calculations was also close to that obtained in XRD patterns (d_{100} = 0.211 nm). A HRTEM image of G-*h*-BN is shown in Figure 4e, and a hexagonal structure can be observed. The distance between the two neighboring bright reflections was 0.251 nm, perfectly corresponding to that in the B−B or N−N atom separations in *h*-BN.[60] XRD patterns of G-*h*-BN and IL/G-*h*-BN are presented in Figure 4f, and the results demonstrated that all the peaks of the *h*-BN and IL/*h*-BN samples were readily indexed to the standard hexagonal phase of *h*-BN (JCPDS Card No. 34-0421). Moreover, the two main peaks still could be found in the XRD pattern of IL/*h*-BN, proving that the structure of *h*-BN was not destroyed after *h*-BN was supported with IL.

FT-IR spectra of G-*h*-BN, IL and IL/G-*h*-BN are listed in Figure 5. For G-*h*-BN (Figure 5a), the adsorption band centered around 1382 cm^{-1} was attributed to in-plane B−N transverse optional modes of hexagonal boron nitride.[61] The last peak 804 cm^{-1} was N−B stretching vibration modes.[62] FT-IR spectrum of IL is depicted in Figure 5b. The bands at 976, 890 and 814 cm^{-1} were due to the vibrations of W−O, W−O−W (octahedral corner-sharing) and W−O−W (octahedral edge-sharing), respectively.[63] The peak around 2920 cm^{-1} was ascribed to C−H stretching vibration. The FT-IR spectrum of IL/G-*h*-BN is presented in Figure 5c. The bands of IL and G-*h*-BN could still be detected, but the intensity of peaks at 975 and 812 cm^{-1} were too weak to be found, which may result from that the amount of IL loaded onto G-*h*-BN was very low.

dx.doi.org/10.1021/sc5006928 | ACS Sustainable Chem. Eng. 2015, 3, 186−194

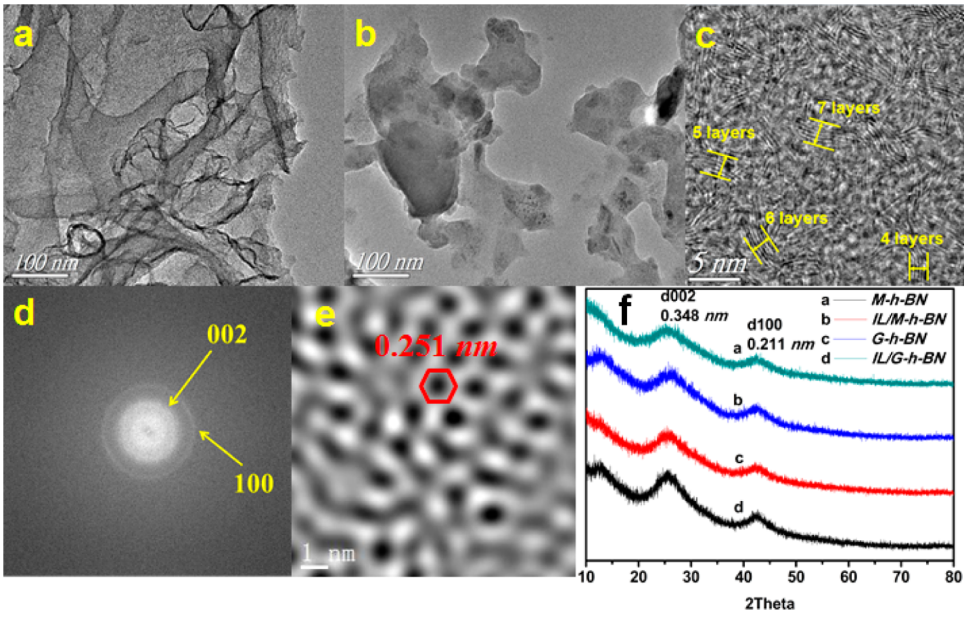

Figure 4. TEM images and XRD pattern of G-*h*-BN and IL/G-*h*-BN (a) TEM image of G-*h*-BN; (b) TEM image of IL/G-*h*-BN; (c) HRTEM of G-*h*-BN; (d) FFT image of panel c; (e) HRTEM image of G-*h*-BN; (f) XRD pattern of *h*-BN and IL/*h*-BN.

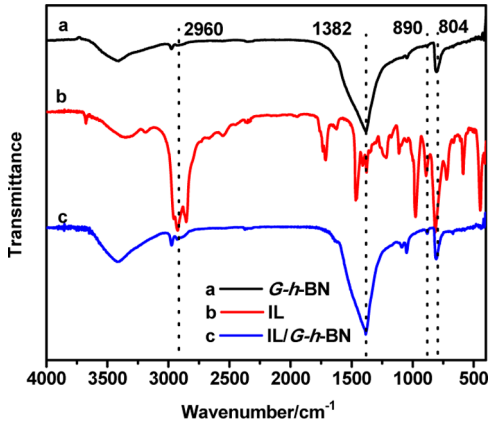

Figure 5. FT-IR spectra of G-*h*-BN(a), IL(b) and IL/G-*h*-BN(c).

Ultraviolet−visible diffuse reflectance spectra (UV-DRS) of G-*h*-BN, IL and IL/G-*h*-BN are presented in Figure 6. A broad peak between 360 and 305 nm of IL was presented (Figure 6a), whereas a sharp peak at 240 nm was found in the spectrum of G-*h*-BN (Figure 6c). The two peaks were also found in the DRS of IL/G-*h*-BN (Figure 6b), proving that G-*h*-BN had been supported with IL fatherly. The band gap energy of BN was calculated based on UV-DRS and discussed in detail, which was an important method to clarify the crystal form of *h*-BN. (Figure S1, Supporting Information) The calculated value of as-prepared BN was 5.25 eV, further proving that this BN was a hexagonal phase.[64]

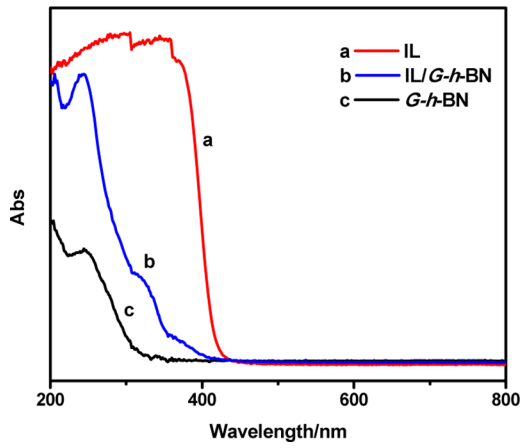

Figure 6. UV-DRS spectra of (a) IL; (b) IL/G-*h*-BN; (c) G-*h*-BN.

Investigation of Desulfurization Efficiency and Reaction Mechanism. The different desulfurization experiments were carried out using DBT-containing *n*-octane as model oil and with H_2O_2 as the oxidant. DBT was selected as an aromatic sulfur compound representative for it was one of the main refractory sulfur-containing compounds in the HDS treatment. Adsorptive desulfurization of 0.05 g of G-*h*-BN, M-*h*-BN and commercial bulk BN is listed in Table 1 and sulfur removal was

Table 1. Sulfur Removal of Different Desulfurization Systems[a]

entry	reaction system	sulfur removal (%)	TOF (h^{-1})[b]
1	G-*h*-BN	39.4	
2	M-*h*-BN	32.5	
3	commercial bulk BN	2.0	
4	IL/G-*h*-BN	26.3	
5	IL/G-*h*-BN+H_2O_2	99.3	27.7
6	IL+H_2O_2	10.6[c]/93.5[d]	2.9/0.32
7	IL+G-*h*-BN+H_2O_2	47.4	
8	IL/M-*h*-BN+H_2O_2	53.5	15.0
9	IL/commercial bulk BN+H_2O_2	7.7	2.1

[a] T = 30 °C, m (catalyst) = 0.05 g, t = 80 min, n (O)/n (S) = 4.0, V (oil) = 5 mL. [b] The catalyst is based on IL. [c] T = 30 °C, m (catalyst) = 0.005 g (this mass equals with the amount of IL in 0.05 g IL/G-*h*-BN), n (O)/n (S) = 4.0, V (oil) = 5 mL. [d] T = 40 °C, m (catalyst) = 0.4 g n (O)/n (S) = 6.0, V (oil) = 5 mL; model oil, 500 ppm DBT; M-*h*-BN, multilayers *h*-BN; G-*h*-BN, graphene-analogue *h*-BN; IL, $[(C_6H_{13})_3PC_{14}H_{29}]_2W_6O_{19}$.

dx.doi.org/10.1021/sc5006928 | ACS Sustainable Chem. Eng. 2015, 3, 186−194

Scheme 1. Proposed Mechanism of Oxidation of DBT on IL/G-*h*-BN

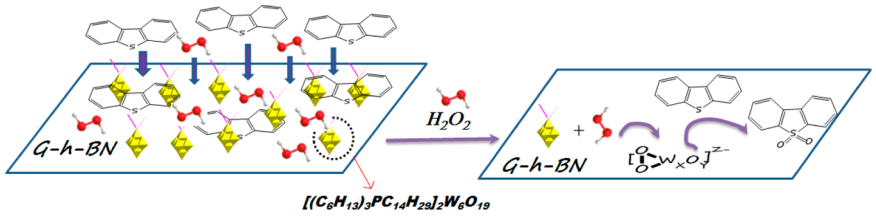

39.4%, 32.5% and 2.0%, respectively. The enhancement of adsorptive desulfurization of G-*h*-BN may be attributed to the higher specific surface area. When G-*h*-BN was supported with IL, adsorptive desulfurization of IL/G-*h*-BN decreased to 26.3%, which may result from the decrease of specific surface area and some adsorptive active sites were occupied by IL. Notably, with addition of H_2O_2 in the heterogeneous IL/G-*h*-BN reaction system, sulfur removal rose significantly, reaching 99.3% (TOF = 27.7). However, sulfur removal of homogeneous equal catalysts of ILs themselves (0.005 g) was only 10.6% and TOF was only 2.9 under the same reaction conditions, revealing that the sulfur removal in IL/G-*h*-BN heterogeneous catalysts improved greatly than that in the IL homogeneous system. After optimizing the reaction conditions, with 0.4 g IL, H_2O_2 and DBT with a molar ratio of 6:1 and 40 °C reaction temperature, 93.5% sulfur removal was also achieved. However, in this IL homogeneous system and reaction temperature, the amount of IL and H_2O_2 increased remarkably and TOF was only 0.32. The usage amount of IL was 80-fold as that of heterogeneous IL/G-*h*-BN. Notably, TOF of IL/G-*h*-BN reached 27.7, which was not only higher than homogeneous equal catalysts of ILs themselves (2.9 and 0.32) but also superior to the most reported catalysts in Table S1 (Supporting Information). Although IL/G-*h*-BN was a heterogeneous catalyst in oxidative desulfurization, higher catalytic activity was presented compared with the homogeneous catalyst of ILs themselves. Moreover, when the same amount of IL was supported on the M-*h*-BN and commercial bulk BN, only 53.5% and 7.7% sulfur removals were exhibited. These results indicated that G-*h*-BN and IL showed excellent synergetic effects to enhance the catalytic activity, and the number of *h*-BN layers played an important role in oxidative desulfurization. The catalytic activity of few-layer *h*-BN supported with IL was much higher than that of multilayer *h*-BN supported with IL.

It was worth noting that the high activity of IL/G-*h*-BN was not only attributed to the large BET surface of G-*h*-BN and the high dispersion of ionic liquid, but also assigned to the special two-dimensional structure of G-*h*-BN, which can adsorb substrate DBT and oxidant. In this reaction system, G-*h*-BN has a virtual orbital of B, presenting some Lewis acidity.[60] The planar-structure DBT molecules with lone pair electrons in S atom or the occupied π-electrons of DBT π-conjugate system may donate the virtual orbitals of B, which enhanced the surface absorbability of IL/G-*h*-BN with substrates.[65,66] In the same way, H_2O_2 was adsorbed on IL/G-*h*-BN easily and combined with tungsten-based IL to oxidize DBT. We inferred that sulfur compounds and oxidant developed local high concentrations on the IL/G-*h*-BN surface, enhancing the catalytic activity of IL. This proposal could explain that the IL/G-*h*-BN, as a heterogeneous catalyst, presented higher catalytic activity than the homogeneous catalyst of ILs themselves in oxidative desulfurization. In contrast, IL/M-*h*-BN exhibited low catalytic performance, which was ascribed to smaller surface sites. The higher surface not only led to high dispersion of IL but also exposed more active sites of *h*-BN for DBT and H_2O_2 adsorption. The more adsorptive sites are responsible for the higher local concentration of DBT and oxidizing species, leading to the possibility for DBT to contact and react with peroxo species adequately. Simultaneously, once the oxidation of DBT on the surface of IL/G-*h*-BN took place, the unoxidized substrates in the oil phase might be delivered to the surface of IL/G-*h*-BN, which remained high concentration of substrates and oxidant on the surface of catalyst and was another contribution to the high catalytic activity. In conclusion, it was synergetic effects of IL and G-*h*-BN that made IL/G-*h*-BN outstanding catalyst for deep oxidative desulfurization. To prove the synergetic effect of IL and G-*h*-BN, we carried out the experiment of desulfurization using a simple mixture of IL and G-*h*-BN. Under the same reaction conditions, the sulfur removal was only 47.4%, which was lower than that of the IL/G-*h*-BN catalyst.

On the basis of the above discussions, we proposed the reaction mechanism in Scheme 1. We found that the oxidative desulfurization initiated with adsorption of H_2O_2 and DBT over the surface of IL/G-*h*-BN subsequently or simultaneously. H_2O_2 reacted with $W_6O_{19}^{2-}$ to form corresponding peroxo species $[W_xO_y(O)_2]^{z-}$,[56] then the peroxo species further reacted with adjacent adsorbed DBT on the surface of IL/G-*h*-BN. After the products desorbed from the surface of IL/G-*h*-BN, the catalyst could be recovered and reused in the following adsorption-oxidation reactions.

To further prove the mechanism of adsorption and catalytic oxidative desulfurization, sulfur compounds in model oil and in catalyst phase were measured by GC−MS. After reaction, the upper phase (model oil) was withdrawn and analyzed directly by GC−MS, whereas the catalyst phase was re-extracted by tetrachloromethane, and then the obtained tetrachloromethane solution was tested by GC−MS. The remnant sulfur species in the model oil were only DBT and there were no oxidized sulfur species, which could be proved by GC−MS. (Figure 7). As for the sulfur species in the catalyst phase, the results showed that DBT and $DBTO_2$ were detected (Figure 8). These results proved that DBT was adsorbed onto the surface of G-*h*-BN first and then was oxidized, which agreed with the mechanism of adsorption and catalytic oxidative desulfurization.

Optimization of Oxidative Desulfurization Parameters. Some factors including the effect of system temperature, reaction time and usage amount of H_2O_2 were investigated in detail because of their importance for the potential industrial process. Figure 9 reveals effects of reaction temperature and time on sulfur removal. In the oxidative desulfurization system, the effect of reaction temperature, such as 20, 30, 40 and 50 °C, was investigated at molar ratio of H_2O_2 and sulfur compound (O/S) = 4:1. The results indicated that sulfur removal was 81.0% after 80 min at 20 °C. It was likely that the oxidation at

dx.doi.org/10.1021/sc5006928 | ACS Sustainable Chem. Eng. 2015, 3, 186−194

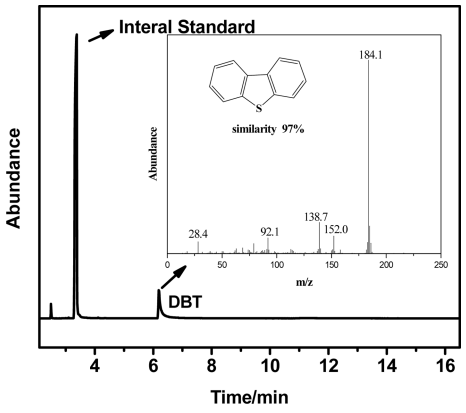

Figure 7. GC−MS analysis of oil phase.

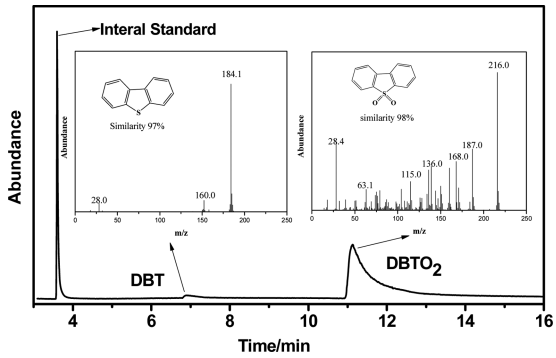

Figure 8. GC−MS analysis of catalyst phase.

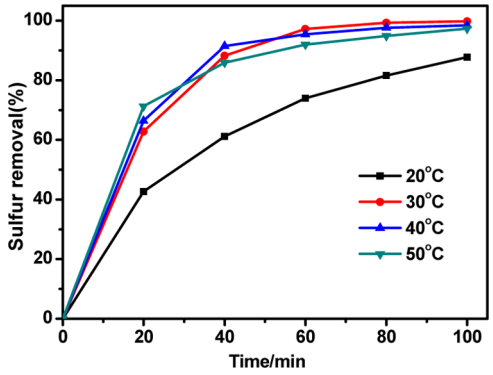

Figure 9. Effects of reaction temperature and time on sulfur removal. Reaction conditions: n (O)/n (S) = 4.0; V (oil) = 5 mL; m (IL/G-h-BN) = 0.0500 g; t = 80 min.

low temperature was limited by kinetics. At a higher reaction temperatures, sulfur removal was enhanced obviously. With the increase of reaction temperature, sulfur removal improved as well during 20 min. However, after 60 min, reaction at 30 °C exhibited the highest activity, which might lie in that H_2O_2 decomposed dramatically at higher temperatures and the utilization of H_2O_2 was low. Therefore, 30 °C was chosen as the most optimiztic reaction temperature, which was efficient and economic. Then, effect of the amount of H_2O_2 was investigated at 30 °C for 80 min. The result of GC chromatogram (Figure S2, Supporting Information) of model oil with different O/S molar ratio showed that when O/S molar ratio increased from 2:1 to 3:1, sulfur content decreased from 140 to 23 ppm. Finally, the O/S molar ratio of 4:1 was chosen as the optimal molar ratio with sulfur residue 3 ppm, which achieved deep desulfurization.

Influence of Different Sulfur-Containing Compounds. Figure 10 presents the influence of different sulfur-containing

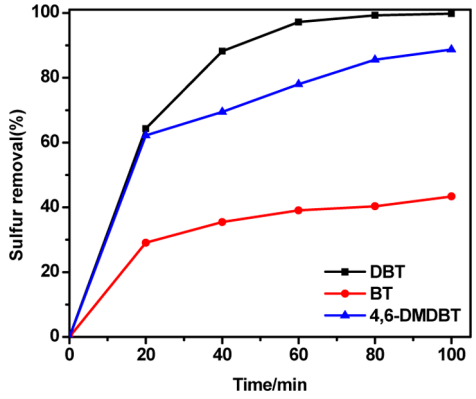

Figure 10. Influence of sulfur-containing compounds. Reaction conditions: T = 30 °C; n (O)/n (S) = 4.0; V (oil) = 5 mL; m (IL/G-h-BN) = 0.0500 g; t = 80 min.

compounds. In the desulfurization system, the feature of the substrates is of great importance in affecting the sulfur removal. Herein, DBT and another two inflexible substrates 4,6-dimethyldibenzothiophene (4,6-DMDBT) and benzothiophene (BT) were investigated. The removal of DBT, BT and 4,6-DMDBT was 99.8%, 43.4% and 88.7% after 100 min, respectively. The oxidative activity decreased in the following order: DBT > 4,6-DMDBT > BT. This order agreed well with the reported polyoxometalate-based catalysts.[61,62] On the basis of the experimental data and references,[50,67,68] we inferred that the reactivity of sulfur-containing compounds was affected synergistically by two facets. For one thing, IL/G-h-BN showed different adsorption capabilities to three sulfur compounds, following the order of DBT > 4,6-DMDBT > BT. The higher adsorption capability produced the higher concentration of substrates on the surface of the catalyst, which was a benefit for the catalytic activity. Also, sulfur compounds' electron density as well as the steric hindrance around the sulfur atoms affected catalytic activity. The electron density of DBT, BT and 4,6-DMDBT was 5.758, 5.739 and 5.760, respectively.[67] The electron density on the sulfur atom of BT is the lowest, leading to the low reactivity. For DBT and 4,6-DMDBT, the electron density on the sulfur is very close. Therefore, reactivity of DBT > 4,6-DMDBT was mainly affected by the steric hindrance of the methyl groups. Based on the previous research, it was relatively easy for BT to be removed from fuels by hydrodesulfurization (HDS), but DBT and 4,6-DMDBT were refractory in HDS. Therefore, this oxidative desulfurization system may be a complementary method to HDS.

Recycling of the Catalyst. The recycling performance for IL/G-h-BN was investigated on the removal of DBT in model oil. No additional treatment was made between the repetitive runs and the recycling of this catalyst was easy to implement. After the first reaction, the solid phase could be separated by centrifugation. After separation, the solid phase was heated to remove the residual oil and H_2O_2. Then, fresh H_2O_2 and model oil were poured into the reactor for the next reaction. After recycling for five times, sulfur removal decreased from 99.3% to 93.4% (Table 2). The result indicated that the desulfurization system could be recycled 5 times with a little decrease in

dx.doi.org/10.1021/sc5006928 | ACS Sustainable Chem. Eng. 2015, 3, 186−194

Table 2. Recycling of the Catalyst

recycle times	1	2	3	4	5
sulfur removal (%)	99.3	99.2	96.1	96.3	93.4

Reaction conditions: T = 30 °C; n (O)/n (S) = 4.0; V (oil) = 5 mL; m (catalyst) = 0.0500 g; t = 80 min.

desulfurization activity. With more recycling times, more and more precipitation ($DBTO_2$) was separated from oil phase, which achieved removing sulfur compounds from oil. We postulate that $DBTO_2$ isolates possibly cover some active species of IL/G-*h*-BN, leading to a little reduction in sulfur removal.

Analysis of the Fresh Catalyst and the Recycled Catalyst. FT-IR, XRD and UV−DRS characterizations were taken to research the fresh catalyst and recycled catalyst. The FT-IR results are listed in Figure 11. There was no change in

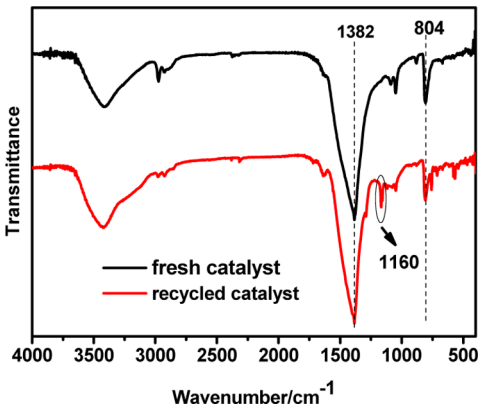

Figure 11. FT-IR spectra of fresh catalyst and recycled catalyst.

the structures of fresh IL/G-*h*-BN and recycled IL/G-*h*-BN, and the two main peaks around 804 and 1382 cm^{-1} could still be found. However, it was worth noting that a new peak around 1160 cm^{-1} could be found in recycled catalyst, which could be attributed to the band of S═O. It suggested that the products of oxidized sulfur compounds would be sulfone, and they were adsorbed on the surface of the catalyst. Additionally, in the XRD (Figure 12) and UV−DRS (Figure 13) spectra, compared recycled catalyst with fresh catalyst, the emerging peaks was ascribed to the sulfone of DBT,[69] which was also proved by the above GC−MS analysis. So, these results further demonstrated the mechanism of adsorption and catalytic oxidative desulfurization.

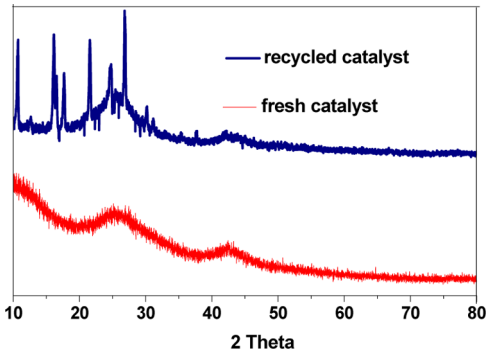

Figure 12. XRD spectra of fresh catalyst and recycled catalyst.

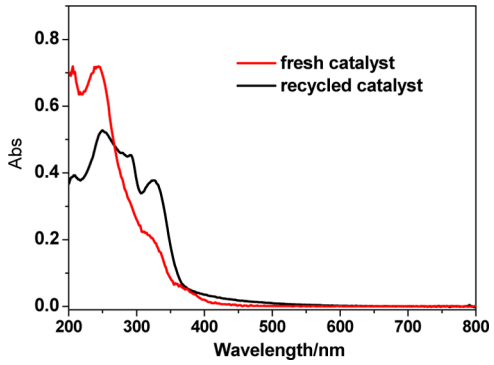

Figure 13. UV−DRS spectra of fresh catalyst and recycled catalyst.

CONCLUSIONS

In summary, we have successfully designed a novel graphene-analogue hexagonal boron nitride as a thermostable and chemically stable support coated with tungsten-based ionic liquid and explored its application in adsorption combined with catalytic oxidative desulfurization system. The reaction condition was very mild and sulfur removal of DBT-containing model oil could reach 99.3% at 30 °C. The graphene-analogue *h*-BN supported with ionic liquid exhibited much higher catalytic activity than multilayer *h*-BN supported with ionic liquid. The recovered IL/G-*h*-BN could be recycled for five times without significant loss of catalytic efficiency. GC−MS and FT-IR were employed to research and validate the reaction mechanism and reaction products. This work also provided a new strategy of designing high activity heterogeneous catalysts for other organic reactions, such as esterification, epoxidation reaction and so on.

ASSOCIATED CONTENT

Supporting Information

Different ionic liquid-based catalytic systems parameters in oxidation of DBT, band gap energy of G-*h*-BN, and effects of O/S molar ratio. This material is available free of charge via the Internet at http://pubs.acs.org.

AUTHOR INFORMATION

Corresponding Authors

*E-mail: zhuws@ujs.edu.cn (W. S. Zhu).
*E-mail: lhm@ujs.edu.cn (H. M. Li).

Notes

The authors declare no competing financial interest.

ACKNOWLEDGMENTS

We thank the National Nature Science Foundation of China (Nos. 21376111, 21276117, 21106055) and the Natural Science Foundation of Jiangsu Province (BK20131207).

REFERENCES

(1) Rogers, R. D.; Seddon, K. R. Ionic liquids - Solvents of the future? *Science* **2003**, *302*, 792−793.
(2) Alvim, H. G. O.; de Lima, T. B.; de Oliveira, H. C. B.; Gozzo, F. C.; de Macedo, J. L.; Abdenur, P. V.; Silva, W. A.; Neto, B. A. D. Ionic Liquid Effect over the Biginelli reaction under homogeneous and heterogeneous catalysis. *ACS Catal.* **2013**, *3*, 1420−1430.
(3) Zhu, W. S.; Zhu, G. P.; Li, H. M.; Chao, Y. H.; Chang, Y. H.; Chen, G. Y.; Han, C. R. Oxidative desulfurization of fuel catalyzed by metal-based surfactant-type ionic liquids. *J. Mol. Catal. A: Chem.* **2011**, *347*, 8−14.

(4) Zhu, W. S.; Huang, W. L.; Li, H. M.; Zhang, M.; Jiang, W.; Chen, G. Y.; Han, C. R. Polyoxometalate-based ionic liquids as catalysts for deep desulfurization of fuels. *Fuel Process. Technol.* **2011**, *92*, 1842−1848.
(5) Giernoth, R. Ionic liquids with a twist: New routes to liquid salts. *Angew. Chem., Int. Ed.* **2010**, *49*, 5608−5609.
(6) Li, F. T.; Kou, C. G.; Sun, Z. M.; Hao, Y. J.; Liu, R. H.; Zhao, D. S. Deep extractive and oxidative desulfurization of dibenzothiophene with $C_5H_9NO{\cdot}SnCl_2$ coordinated ionic liquid. *J. Hazard. Mater.* **2012**, *205*, 164−170.
(7) Mehnert, C. P.; Cook, R. A.; Dispenziere, N. C.; Afeworki, M. Supported ionic liquid catalysis - A new concept for homogeneous hydroformylation catalysis. *J. Am. Chem. Soc.* **2002**, *124*, 12932−12933.
(8) Chen, X. L.; Souvanhthong, B.; Wang, H.; Zheng, H. W.; Wang, X. H.; Huo, M. X. Polyoxometalate-based ionic liquid as thermo-regulated and environmentally friendly catalyst for starch oxidation. *Appl. Catal., B* **2013**, *138*, 161−166.
(9) Leng, Y.; Zhao, J. W.; Jiang, P. P.; Wang, J. Amphiphilic polyoxometalate-paired polymer coated Fe_3O_4: Magnetically recyclable catalyst for epoxidation of bio-derived olefins with H_2O_2. *ACS Appl. Mater. Interfaces* **2014**, *6*, 5947−5954.
(10) Zhang, Z. F.; Xie, Y.; Li, W. J.; Hu, S. Q.; Song, J. L.; Jiang, T.; Han, B. X. Hydrogenation of carbon dioxide is promoted by a task-specific ionic liquid. *Angew. Chem., Int. Ed.* **2008**, *47*, 1127−1129.
(11) Cui, G. K.; Zheng, J. J.; Luo, X. Y.; Lin, W. J.; Ding, F.; Li, H.; Wang, C. Tuning anion-functionalized ionic liquids for improved SO_2 capture. *Angew. Chem., Int. Ed.* **2013**, *52*, 10620−10624.
(12) Zhu, W. S.; Li, H. M.; Gu, Q. Q.; Wu, P. W.; Zhu, G. P.; Yan, Y. S.; Chen, G. Y. Kinetics and mechanism for oxidative desulfurization of fuels catalyzed by peroxo-molybdenum amino acid complexes in water-immiscible ionic liquids. *J. Mol. Catal. A: Chem.* **2011**, *336*, 16−22.
(13) Wang, X. T.; Chen, W.; Song, Y. F. Directional self-assembly of exfoliated layered europium hydroxide nanosheets and $Na_9EuW_{10}O_{36}{\cdot}32H_2O$ for application in desulfurization. *Eur. J. Inorg. Chem.* **2014**, *2014*, 2779−2786.
(14) Chi, Y. S.; Li, C. P.; Jiao, Q. Z.; Liu, Q. S.; Yan, P. F.; Liu, X. M.; Welz-Biermann, U. Desulfurization by oxidation combined with extraction using acidic room-temperature ionic liquids. *Green Chem.* **2011**, *13*, 1224−1229.
(15) Xiong, J.; Zhu, W. S.; Li, H. M.; Xu, Y. H.; Jiang, W.; Xun, S. H.; Liu, H.; Zhao, Z. Immobilized Fenton-like ionic liquid: Catalytic performance for oxidative desulfurization. *AIChE J.* **2013**, *59*, 4696−4704.
(16) Nie, Y.; Li, C. X.; Sun, A. J.; Meng, H.; Wang, Z. H. Extractive desulfurization of gasoline using imidazolium-based phosphoric ionic liquids. *Energy Fuel* **2006**, *20*, 2083−2087.
(17) Gao, H. S.; Luo, M. F.; Xing, J. M.; Wu, Y.; Li, Y. G.; Li, W. L.; Liu, Q. F.; Liu, H. Z. Desulfurization of fuel by extraction with pyridinium-based ionic liquids. *Ind. Eng. Chem. Res.* **2008**, *47*, 8384−8388.
(18) Zhao, D. S.; Sun, Z. M.; Li, F.; Liu, R.; Shan, H. D. Oxidative desulfurization of thiophene catalyzed by $(C_4H_9)_4NBr{\cdot}2C_6H_{11}NO$ coordinated ionic liquid. *Energy Fuel* **2008**, *22*, 3065−3069.
(19) Jiang, Y. Q.; Zhu, W. S.; Li, H. M.; Yin, S.; Liu, H.; Xie, Q. J. Oxidative Desulfurization of fuels catalyzed by Fenton-like ionic liquids at room temperature. *ChemSusChem* **2011**, *4*, 399−403.
(20) Lissner, E.; de Souza, W. F.; Ferrera, B.; Dupont, J. Oxidative desulfurization of fuels with task-specific ionic liquids. *ChemSusChem* **2009**, *2*, 962−964.
(21) Schneider, M. J.; Haumann, M.; Stricker, M.; Sundermeyer, J.; Wasserscheid, P. Gas-phase oxycarbonylation of methanol for the synthesis of dimethyl carbonate using copper-based supported ionic liquid phase (SILP) catalysts. *J. Catal.* **2014**, *309*, 71−78.
(22) Riisager, A.; Fehrmann, R.; Flicker, S.; van Hal, R.; Haumann, M.; Wasserscheid, P. Very stable and highly regioselective supported ionic-liquid-phase (SILP) catalysis: Continuous flow fixed-bed hydroformylation of propene. *Angew. Chem., Int. Ed.* **2005**, *44*, 815−819.
(23) Zhang, Z. M.; Wu, L. B.; Dong, J.; Li, B. G.; Zhu, S. P. Preparation and SO_2 sorption/desorption behavior of an ionic liquid supported on porous silica particles. *Ind. Eng. Chem. Res.* **2009**, *48*, 2142−2148.
(24) Gurkan, B. E.; de la Fuente, J. C.; Mindrup, E. M.; Ficke, L. E.; Goodrich, B. F.; Price, E. A.; Schneider, W. F.; Brennecke, J. F. Equimolar CO_2 absorption by anion-functionalized ionic liquids. *J. Am. Chem. Soc.* **2010**, *132*, 2116−2117.
(25) Liu, F. J.; Wang, L.; Sun, Q.; Zhu, L. F.; Meng, X. J.; Xiao, F. S. Transesterification catalyzed by ionic liquids on superhydrophobic mesoporous polymers: Heterogeneous catalysts that are faster than homogeneous catalysts. *J. Am. Chem. Soc.* **2012**, *134*, 16948−16950.
(26) Shi, F.; Zhang, Q. H.; Li, D. M.; Deng, Y. Q. Silica-gel-confined ionic liquids: A new attempt for the development of supported nanoliquid catalysis. *Chem.—Eur. J.* **2005**, *11*, 5279−5288.
(27) Crudden, C. M.; Sateesh, M.; Lewis, R. Mercaptopropyl-modified mesoporous silica: A remarkable support for the preparation of a reusable, heterogeneous palladium catalyst for coupling reactions. *J. Am. Chem. Soc.* **2005**, *127*, 10045−10050.
(28) Ma, X. M.; Zhou, Y. X.; Zhang, J. C.; Zhu, A. L.; Jiang, T.; Han, B. X. Solvent-free Heck reaction catalyzed by a recyclable Pd catalyst supported on SBA-15 via an ionic liquid. *Green Chem.* **2008**, *10*, 59−66.
(29) Karimi, B.; Elhamifar, D.; Clark, J. H.; Hunt, A. J. Ordered mesoporous organosilica with ionic-liquid framework: An efficient and reusable support for the palladium-catalyzed Suzuki-Miyaura coupling reaction in water. *Chem.—Eur. J.* **2010**, *16*, 8047−8053.
(30) Kohler, F.; Roth, D.; Kuhlmann, E.; Wasserscheid, P.; Haumann, M. Continuous gas-phase desulfurisation using supported ionic liquid phase (SILP) materials. *Green Chem.* **2010**, *12*, 979−984.
(31) Rodriguez-Perez, L.; Pradel, C.; Serp, P.; Gomez, M.; Teuma, E. Supported ionic liquid phase containing palladium nanoparticles on functionalized multiwalled carbon nanotubes: Catalytic materials for sequential Heck coupling/hydrogenation process. *ChemCatChem* **2011**, *3*, 749−754.
(32) Abello, S.; Medina, F.; Rodriguez, X.; Cesteros, Y.; Salagre, P.; Sueiras, J. E.; Tichit, D.; Coq, B. Supported choline hydroxide (ionic liquid) as heterogeneous catalyst for aldol condensation reactions. *Chem. Commun.* **2004**, 1096−1097.
(33) Khan, N. A.; Hasan, Z.; Jhung, S. H. Ionic liquids supported on metal-organic frameworks: Remarkable adsorbents for adsorptive desulfurization. *Chem.—Eur. J.* **2014**, *20*, 376−380.
(34) Rao, C. N. R.; Sood, A. K.; Subrahmanyam, K. S.; Govindaraj, A. Graphene: The new two-dimensional nanomaterial. *Angew. Chem., Int. Ed.* **2009**, *48*, 7752−7777.
(35) Brugger, T.; Ma, H. F.; Iannuzzi, M.; Berner, S.; Winkler, A.; Hutter, J.; Osterwalder, J.; Greber, T. Nanotexture switching of single-layer hexagonal boron nitride on rhodium by intercalation of hydrogen atoms. *Angew. Chem., Int. Ed.* **2010**, *49*, 6120−6124.
(36) Xu, M. S.; Liang, T.; Shi, M. M.; Chen, H. Z. Graphene-like two-dimensional materials. *Chem. Rev.* **2013**, *113*, 3766−3798.
(37) Golberg, D.; Bando, Y.; Huang, Y.; Terao, T.; Mitome, M.; Tang, C. C.; Zhi, C. Y. Boron nitride nanotubes and nanosheets. *ACS Nano* **2010**, *4*, 2979−2993.
(38) Kubota, Y.; Watanabe, K.; Tsuda, O.; Taniguchi, T. Deep ultraviolet light-emitting hexagonal boron nitride synthesized at atmospheric pressure. *Science* **2007**, *317*, 932−934.
(39) Watanabe, K.; Taniguchi, T.; Niiyama, T.; Miya, K.; Taniguchi, M. Far-ultraviolet plane-emission handheld device based on hexagonal boron nitride. *Nat. Photonics* **2009**, *3*, 591−594.
(40) Shi, Y. M.; Hamsen, C.; Jia, X. T.; Kim, K. K.; Reina, A.; Hofmann, M.; Hsu, A. L.; Zhang, K.; Li, H. N.; Juang, Z. Y.; Dresselhaus, M. S.; Li, L. J.; Kong, J. Synthesis of few-layer hexagonal boron nitride thin film by chemical vapor deposition. *Nano Lett.* **2010**, *10*, 4134−4139.
(41) Zhu, W. S.; Zhang, J. T.; Li, H. M.; Chao, Y. H.; Jiang, W.; Yin, S.; Liu, H. Fenton-like ionic liquids/H_2O_2 system: One-pot extraction combined with oxidation desulfurization of fuel. *RSC Adv.* **2012**, *2*, 658−664.

(42) Li, F. T.; Liu, Y.; Sun, Z. M.; Chen, L. J.; Zhao, D. S.; Liu, R. H.; Kou, C. G. Deep extractive desulfurization of gasoline with $xEt_3NHCl{\cdot}FeCl_3$ ionic liquids. *Energy Fuels* **2010**, *24*, 4285−4289.
(43) Yu, G. R.; Zhao, J. J.; Song, D. D.; Asumana, C.; Zhang, X. Y.; Chen, X. C. Deep oxidative desulfurization of diesel fuels by acidic ionic liquids. *Ind. Eng. Chem. Res.* **2011**, *50*, 11690−11697.
(44) Kong, L. Y.; Li, G.; Wang, X. S.; Wu, B. Oxidative desulfurization of organic sulfur in gasoline over Ag/TS-1. *Energy Fuels* **2006**, *20*, 896−902.
(45) Zhao, D. S.; Liu, R.; Wang, J. L.; Liu, B. Y. Photochemical oxidation-ionic liquid extraction coupling technique in deep desulphurization of light oil. *Energy Fuels* **2008**, *22*, 1100−1103.
(46) Zhang, H. X.; Gao, J. J.; Meng, H.; Li, C. X. Removal of thiophenic sulfurs using an extractive oxidative desulfurization process with three new phosphotungstate catalysts. *Ind. Eng. Chem. Res.* **2012**, *51*, 6658−6665.
(47) Xiao, J.; Wu, L. M.; Wu, Y.; Liu, B.; Dai, L.; Li, Z.; Xia, Q. B.; Xi, H. X. Effect of gasoline composition on oxidative desulfurization using a phosphotungstic acid/activated carbon catalyst with hydrogen peroxide. *Appl. Energy* **2014**, *113*, 78−85.
(48) Sundararaman, R.; Song, C. S. Catalytic oxidative desulfurization of diesel fuels using air in a two-step approach. *Ind. Eng. Chem. Res.* **2014**, *53*, 1890−1899.
(49) Lv, H. Y.; Ren, W. Z.; Liao, W. P.; Chen, W.; Li, Y.; Suo, Z. H. Aerobic oxidative desulfurization of model diesel using a B-type Anderson catalyst $[(C_{18}H_{37})_2N(CH_3)_2]_3Co(OH)_6Mo_6O_{18}{\cdot}3H_2O$. *Appl. Catal., B* **2013**, *138*, 79−83.
(50) Kim, T. W.; Kim, M. J.; Kleitz, F.; Nair, M. M.; Guillet-Nicolas, R.; Jeong, K. E.; Chae, H. J.; Kim, C. U.; Jeong, S. Y. Tailor-made mesoporous Ti-SBA-15 catalysts for oxidative desulfurization of refractory aromatic sulfur compounds in transport fuel. *ChemCatChem* **2012**, *4*, 687−697.
(51) Zhang, W.; Zhang, H.; Xiao, J.; Zhao, Z. X.; Yu, M.; Li, Z. Carbon nanotube catalysts for oxidative desulfurization of a model diesel fuel using molecular oxygen. *Green Chem.* **2014**, *16*, 211−220.
(52) Li, F. T.; Liu, R. H.; Wen, J. H.; Zhao, D. S.; Sun, Z. M.; Liu, Y. Desulfurization of dibenzothiophene by chemical oxidation and solvent extraction with $Me_3NCH_2C_6H_5Cl{\cdot}2ZnCl_2$ ionic liquid. *Green Chem.* **2009**, *11*, 883−888.
(53) Zhu, W. S.; Wu, P. W.; Yang, L.; Chang, Y. H.; Chao, Y. H.; Li, H. M.; Jiang, Y. Q.; Jiang, W.; Xun, S. H. Pyridinium-based temperature-responsive magnetic ionic liquid for oxidative desulfurization of fuels. *Chem. Eng. J.* **2013**, *229*, 250−256.
(54) Zhang, M.; Zhu, W. S.; Xun, S. H.; Li, H. M.; Gu, Q. Q.; Zhao, Z.; Wang, Q. Deep oxidative desulfurization of dibenzothiophene with POM-based hybrid materials in ionic liquids. *Chem. Eng. J.* **2013**, *220*, 328−336.
(55) Nag, A.; Raidongia, K.; Hembram, K.; Datta, R.; Waghmare, U. V.; Rao, C. N. R. graphene analogues of BN: Novel synthesis and properties. *ACS Nano* **2010**, *4*, 1539−1544.
(56) Zhu, W. S.; Ding, Y. X.; Li, H. M.; Qin, J.; Chao, Y. H.; Xiong, J.; Xu, Y. H.; Liu, H. Application of a self-emulsifiable task-specific ionic liquid in oxidative desulfurization of fuels. *RSC Adv.* **2013**, *3*, 3893−3898.
(57) Ismach, A.; Chou, H.; Ferrer, D. A.; Wu, Y.; McDonnell, S.; Floresca, H. C.; Covacevich, A.; Pope, C.; Piner, R.; Kim, M. J.; Wallace, R. M.; Colombo, L.; Ruoff, R. S. Toward the controlled synthesis of hexagonal boron nitride films. *ACS Nano* **2012**, *6*, 6378−6385.
(58) Song, L.; Ci, L. J.; Lu, H.; Sorokin, P. B.; Jin, C. H.; Ni, J.; Kvashnin, A. G.; Kvashnin, D. G.; Lou, J.; Yakobson, B. I.; Ajayan, P. M. Large scale growth and characterization of atomic hexagonal boron nitride layers. *Nano Lett.* **2010**, *10*, 3209−3215.
(59) Gorbachev, R. V.; Riaz, I.; Nair, R. R.; Jalil, R.; Britnell, L.; Belle, B. D.; Hill, E. W.; Novoselov, K. S.; Watanabe, K.; Taniguchi, T. Hunting for monolayer boron nitride: Optical and Raman signatures. *Small* **2011**, *7*, 465−468.
(60) Zhi, C. Y.; Bando, Y.; Tang, C. C.; Kuwahara, H.; Golberg, D. Large-scale fabrication of boron nitride nanosheets and their utilization in polymeric composites with improved thermal and mechanical properties. *Adv. Mater.* **2009**, *21*, 2889−2893.
(61) Tang, C. C.; Bando, Y.; Sato, T.; Kurashima, K. Uniform boron nitride coatings on silicon carbide nanowires. *Adv. Mater.* **2002**, *14*, 1046−1049.
(62) Wang, X. B.; Zhi, C. Y.; Li, L.; Zeng, H. B.; Li, C.; Mitome, M.; Golberg, D.; Bando, Y. "Chemical Blowing" of thin-walled bubbles: High-throughput fabrication of large-area, few-layered BN and C-x-BN nanosheets. *Adv. Mater.* **2011**, *23*, 4072−4076.
(63) Ding, Y. X.; Zhu, W. S.; Li, H. M.; Jiang, W.; Zhang, M.; Duan, Y. Q.; Chang, Y. H. Catalytic oxidative desulfurization with a hexatungstate/aqueous H_2O_2/ionic liquid emulsion system. *Green Chem.* **2011**, *13*, 1210−1216.
(64) Gao, G. H.; Gao, W.; Cannuccia, E.; Taha-Tijerina, J.; Balicas, L.; Mathkar, A.; Narayanan, T. N.; Liu, Z.; Gupta, B. K.; Peng, J.; Yin, Y. S.; Rubio, A.; Ajayan, P. M. Artificially stacked atomic layers: Toward new van der Waals solids. *Nano Lett.* **2012**, *12*, 3518−3525.
(65) Lin, Y.; Williams, T. V.; Cao, W.; Elsayed-Ali, H. E.; Connell, J. W. Defect functionalization of hexagonal boron nitride nanosheets. *J. Phys. Chem. C* **2010**, *114*, 17434−17439.
(66) Huang, C. J.; Ye, W. Q.; Liu, Q. W.; Qiu, X. Q. Dispersed Cu_2O octahedrons on h-BN nanosheets for *p*-nitrophenol reduction. *ACS Appl. Mater. Interfaces* **2014**, *6*, 14469−14476.
(67) Zhu, W. S.; Li, H. M.; Jiang, X.; Yan, Y. S.; Lu, J. D.; He, L. N.; Xia, J. Commercially available molybdic compound-catalyzed ultra-deep desulfurization of fuels in ionic liquids. *Green Chem.* **2008**, *10*, 641−646.
(68) Xu, J. H.; Zhao, S.; Chen, W.; Wang, M.; Song, Y. F. Highly efficient extraction and oxidative desulfurization system using $Na_7H_2LaW_{10}O_{36}{\cdot}32H_2O$ in $[bmim]BF_4$ at Room Temperature. *Chem.—Eur. J.* **2012**, *18*, 4775−4781.
(69) Castillo, K.; Parsons, J. G.; Chavez, D.; Chianelli, R. R. Oxidation of dibenzothiophene to dibenzothiophene-sulfone using silica gel. *J. Catal.* **2009**, *268*, 329−334.